# STATISTICAL CHARACTERISTICS OF LEAKED AKR OBSERVED AT SOUTH POLE STATION, ANTARCTICA

J. LaBelle<sup>1\*</sup> , and N. Schwartz<sup>1</sup>

\*Corresponding author: James.W.LaBelle@dartmouth.edu

### Citation:

LaBelle & Schwartz, 2023, Statistical characteristics of leaked AKR observed at South Pole Station, Antarctica, in Planetary, Solar and Heliospheric Radio Emissions IX, editors: Fischer, G., Jackman, C. M., Louis, C. K., Sulaiman, A. H., Zucca, P., doi: 10.25546/103087

### Abstract

There is mounting evidence of a component of terrestrial auroral kilometric radiation (AKR) that is converted to whistler mode and radiated downward toward the planet, observable even at ground level. Three years of data from South Pole Station in 2018–2020 provide statistics of characteristics of leaked AKR at ground level. The events occur in an approximately 90-day interval around winter solstice, apparently requiring darkness in the ionosphere to be observed at ground level. They favor pre-midnight/midnight magnetic local times, which is consistent with the connection of AKR, observed in space, to auroral substorms. The frequency distribution of ground-level AKR is truncated compared to that observed in space, with primarily the higher end of the frequency range being observed, 400–600 kHz, corresponding to the low altitude range of source heights, 2500–3500 km, assuming generation at the electron cyclotron frequency. Approximately half of the events have maximum radiance exceeding  $1.5 \times 10^{-18}$  W/m<sup>2</sup>/Hz, with the strongest events exceeding 10<sup>-16</sup> W/m<sup>2</sup>/Hz; these intensities are up to two orders of magnitude lower than those observed in the ionosphere, suggesting that most of the leaked AKR is at large wave normal angles that cannot penetrate the Earth-ionosphere boundary.

<sup>&</sup>lt;sup>1</sup>Department of Physics and Astronomy, Dartmouth College, Hanover, New Hampshire, USA

### 1 Introduction

Auroral kilometric radiation (AKR) is of two main types, escaping and leaked. Escaping AKR is better known, first described by Gurnett (1974). It is primarily X-mode radiation, though partly O-mode, and is beamed away from Earth from sources in the auroral acceleration region. The generation mechanism is the electron cyclotron maser resulting from the "horseshoe" distribution of auroral electrons that develops in the acceleration region, which in the lowest density regions generates X-mode at frequencies close to the electron cyclotron frequency and wave-vectors perpendicular to the magnetic field (Pritchett et al., 1999; reviews by Ergun et al., 2000 and Treumann, 2006). The mechanism is extremely efficient, at times converting up to one percent of the auroral energy into radio waves detectable by satellites at great distances. Less well known is the other type of AKR, called leaked AKR, which was first identified by Oya et al. (1979). Leaked AKR is whistler mode radiation in the same frequency range as escaping AKR, but observed at low altitudes well below the auroral acceleration region with low Earth orbit satellites (Oya et al., 1985; Shutte et al., 1997; Parrot & Berthelier, 2012; Parrot et al., 2022), sounding rockets (Morioka et al., 1988; LaBelle et al., 1999), and ground-based instruments (LaBelle et al., 1999; LaBelle & Anderson, 2011; LaBelle et al., 2015, 2022). It is distinguished from whistler mode auroral hiss, which sometimes occupies the same frequency range, by its longer duration and its fine structures which closely resemble escaping AKR but differ from auroral hiss. Several mechanisms have been proposed for leaked AKR, including ballistic wave transformation (Krasovskiy et al., 1983), nonlinear interaction of auroral Alfvén and Langmuir waves (Chian et al., 1994), and emission and mode conversion of quasi-parallel Z-mode waves at altitudes below the generation of escaping AKR at comparable frequencies (Wu et al., 1989; Ziebell et al., 1991). Another possibility is emission and mode conversion of perpendicular Z-mode waves generated by cyclotron maser in the auroral acceleration region at locations close to or identical with the sources of escaping AKR at comparable frequencies. This last mechanism is similar to early suggestions by Oya et al. (1985) and supported by Cluster observations of Mutel et al. (2011). It seems consistent with the fine structure of leaked AKR (LaBelle et al., 2022), though experimental evidence falls short of proving it, and theoretical work is needed to understand whether the required mode conversion and downward propagation are viable.

Obervations of leaked AKR by low-Earth-orbit satellites and rockets have generally been occasional, not allowing extensive statistical characterization of the emissions. The exception is observations made with the DEMETER (Detection of Electromagnetic Emissions Transmitted from Earthquake Regions) satellite, which were numerous, although the satellite's coverage emphasized latitudes below 65°. These vielded information on magnetic local time, seasonal, longitudinal, and frequency distributions, as well as occurrence rates in both hemispheres, for AKR-like emissions observed in the ionosphere at 660 km (Parrot et al., 2022). Ground-level observations of leaked AKR in the northern hemisphere have been exceedingly rare, with only one event reported in the literature (Figure 3 of LaBelle et al., 1999). However, copious data are available from South Pole Station, where hundreds of events per year have been detected. The lower detection rate of ground-level leaked AKR in the northern hemisphere has been attributed to higher levels of man-made interference masking the natural phenomena, but this hypothesis has not been investigated very deeply or quantitatively and might not explain the extreme difference between observations in the north versus those at South Pole. Mutel et al. (2004) report that escaping AKR is very slightly more common in the southern hemisphere. However, Parrot et al. (2022) report that leaked AKR observed above the ionosphere is 30% more common in the northern hemisphere. Recently, Arase satellite data reveal interhemispheric asymmetries in magnetic local time and frequency range of escaping AKR propagating to mid-latitudes (Xiao et al., 2022). It remains unclear the degree to which these discrepancies result from interhemispheric asymmetry in auroral current systems, AKR generation and propagation, or interference issues affecting measurements.

This paper presents statistical characterizations of leaked AKR at ground–level based on hundreds of events observed at South Pole during 2018–2020, complementing similar statistical characterizations of leaked AKR in the ionosphere (Parrot et al., 2022) and characterizations of escaping AKR from decades of spacecraft observations (e.g., Fogg et al., 2022, and references therein).

# 2 Data presentation

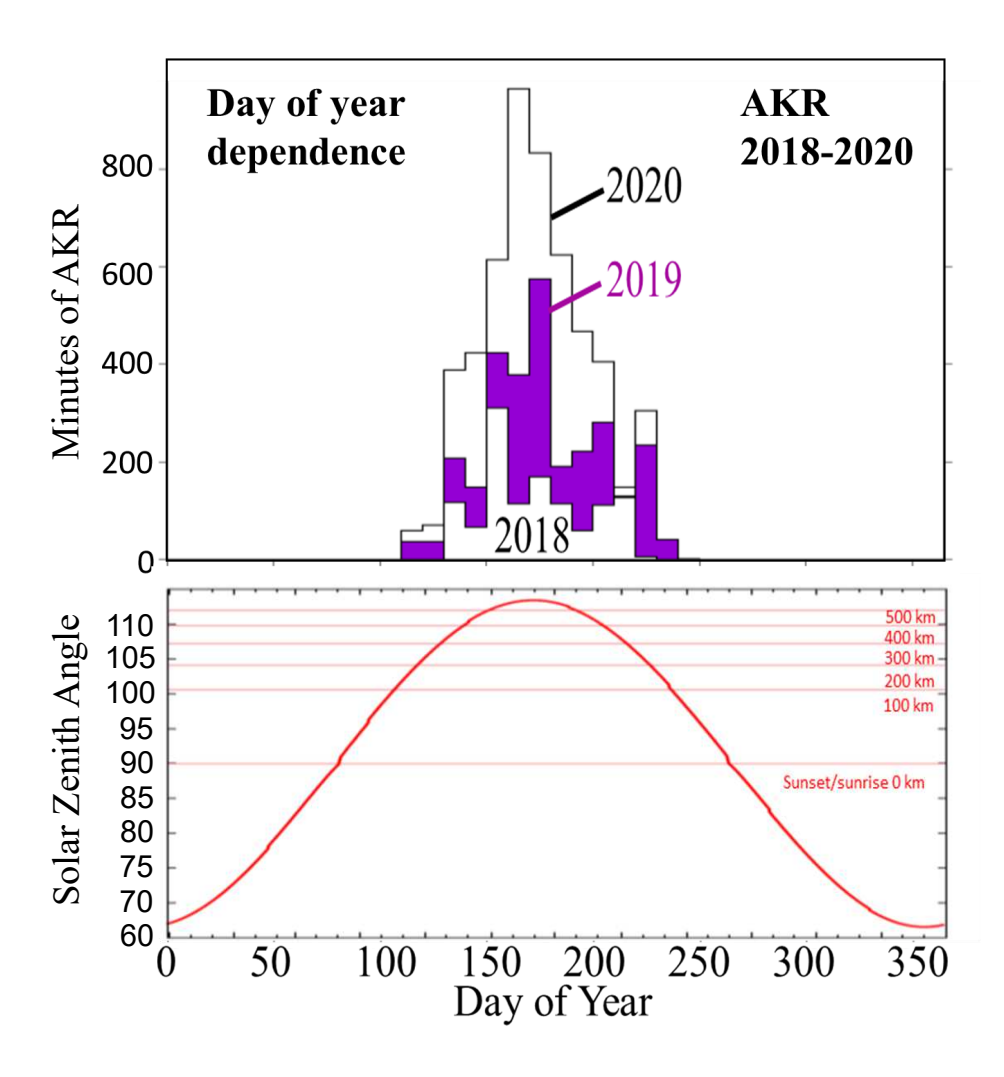


Figure 1: (a) Day of year distribution of leaked AKR observed at South Pole Station in 2018–2020. Leaked AKR occurs roughly between May 20 and August 20 of each year. (b) Solar zenith angle at selected altitudes above South Pole Station as a function of day of year.

Figure 1 shows the day of year distribution of leaked AKR observed at South Pole during 2018–2020. These and subsequent distributions of leaked AKR occurrence are determined from a database of start and end times and upper and lower frequency bounds measured for intervals of AKR identified through manual inspection of summary spectrograms covering 40 minutes and 0–2000 kHz. At South Pole, day of year (doy) is equivalent to solar zenith angle (SZA) which minimizes on December 21 (doy 355), is less than 90° between September and March (doy 266–365 and 1–80), maximizes on June 21 (doy 172), and is greater than 90° between March and September (doy 80–266). A consistent pattern repeats all three years: virtually all leaked AKR at South Pole occurs between about May 20 and August 20. Figure 1b shows SZA at South Pole and sunrise/sunset times as a function of altitude above the station. The turn on (off) dates of leaked AKR correspond to sunset (sunrise) at approximately F–region altitudes. However, there is an asymmetry in that leaked AKR is observed for two months after winter solstice but only one month before; that is, it is observed down to somewhat greater SZA after solstice than before. The international reference ionosphere (IRI–2016) model (Bilitza et al., 2017) suggests that electron density

versus day of year at South Pole is likewise asymmetric around the winter solstice; for 2018–2020, this model predicts minimum F-peak density in August, well past the June solstice. However, the modelled F-peak density is significantly larger in late May than late August, and the modelled E-peak density is uniform for all sun-down dates, so neither F-region nor E-region density alone explains the threshold dates for detection of leaked AKR. The cause of these consistent cutoff dates seems likely related to either trans- or sub-ionospheric propagation conditions, but the detailed mechanism is unclear.

Figure 2a shows the same three years of observations of leaked AKR at South Pole, as a function of time of day (UT). Unlike most locations, at South Pole the time of day is not related to SZA which varies on an annual cycle. Therefore the time–of–day distribution at South Pole relates to magnetic local time (MLT). Midnight MLT is at 0350 UT. Figure 2a shows that leaked AKR favors pre–midnight MLT, occurring primarily in the five–hour interval 23–04 UT (1910–0010 MLT). Ground–based observations alone cannot distinguish the degree to which this distribution characterizes the generation of leaked AKR versus the conditions favorable for its propagation to low altitudes, penetration through the Earth–ionosphere boundary, or subionospheric propagation, all of which could also have MLT dependences. However, a link between leaked AKR generation and substorm activity would not be surprising since escaping AKR is well known to have a connection to substorms (Liou et al., 2000) and in fact has been applied extensively to remotely sense substorm dynamics (Morioka et al., 2007, 2014, and references therein).

Because the MLT distribution in Figure 2a suggests a connection to auroral substorms, it motivates a superposed epoch analysis with respect to substorm onset. The reference time for the analysis is the onset time determined by an algorithm applied to the Supermag magnetometer database (Newell & Gjerloev, 2011a). Onsets determined by this algorithm in 2018–2020 have been screened for geographic longitudes between 235–355 East; that is, within 60° of longitude relative to the location magnetically conjugate to South Pole. Use of conjugate data could possibly complicate interpretation of the results because of the differences in AKR occurrence in the two hemispheres discussed above (e.g., Parrot et al., 2022), but it is required because Supermag has far fewer magnetometers and identifies substorm onsets less effectively in the southern hemisphere. This method yields 244 onset times between May 20 and August 31 in the three years 2018–2020. For each onset time meeting these criteria, presence or absence of leaked AKR is determined for each one-minute interval as a function of time before or after the onset, using the same AKR database obtained from manual inspection of spectrograms as used for the occurrence distributions in Figures 1-2. Figure 2b shows the accumulation of these timing measurements, summed over all of the onsets. Not all of the observed leaked AKR is represented in this plot, only that within six hours of a substorm onset independently determined. Figure 2b suggests a correlation between leaked AKR and substorms, since leaked AKR becomes more prevalent closer to the onset time. Most striking, however, is the evidence that leaked AKR strongly favors pre-onset versus post-onset times. In fact, there is hardly any immediate post-onset leaked AKR; the onset time almost acts as a cutoff for the phenomenon at ground level. This result contrasts with similar analyses of escaping AKR, for which statistical superposed epoch analyses (Waters et al., 2022) and case studies (Morioka et al., 2011) suggest onset of AKR bursts coincident with the substorm expansion phase. While it is possible that generation of leaked AKR favors pre-onset conditions, the most likely explanation for the effective cutoff involves propagation. From the time of onset, electron density is drastically increased over a large portion of the sky, including in the E-region, an effect which likely influences the ability of the leaked AKR to penetrate the Earth-ionosphere boundary to be observed at ground-level. The explanation of the substorm onset cutoff in leaked AKR may therefore be related to the explanation of the time-of-day thresholds found in Figure 1.

Figure 3 shows the frequency distribution of leaked AKR observed at South Pole during the three study years. The bulk of the ground–level leaked AKR occurs between 400 and 600 kHz (59.1% of the one—minute/10–kHz bins), with lesser amounts at 200–400 kHz (20.5%) and 600–850 kHz (20.4%). This distribution is potentially affected by radio frequency interference which at South Pole originates in the station not from broadcast or beacon transmissions. The interference masks certain frequencies and has only a small effect on the distribution as it is binned in Figure 3; it implies an uncertainty of up to 50 kHz in the apparent cutoff frequencies.

Despite this uncertainty, it is clear that leaked AKR observed at South Pole occupies a narrower frequency range than escaping AKR detected with distant satellites; the latter spans primarily 100–600 kHz (Kaiser

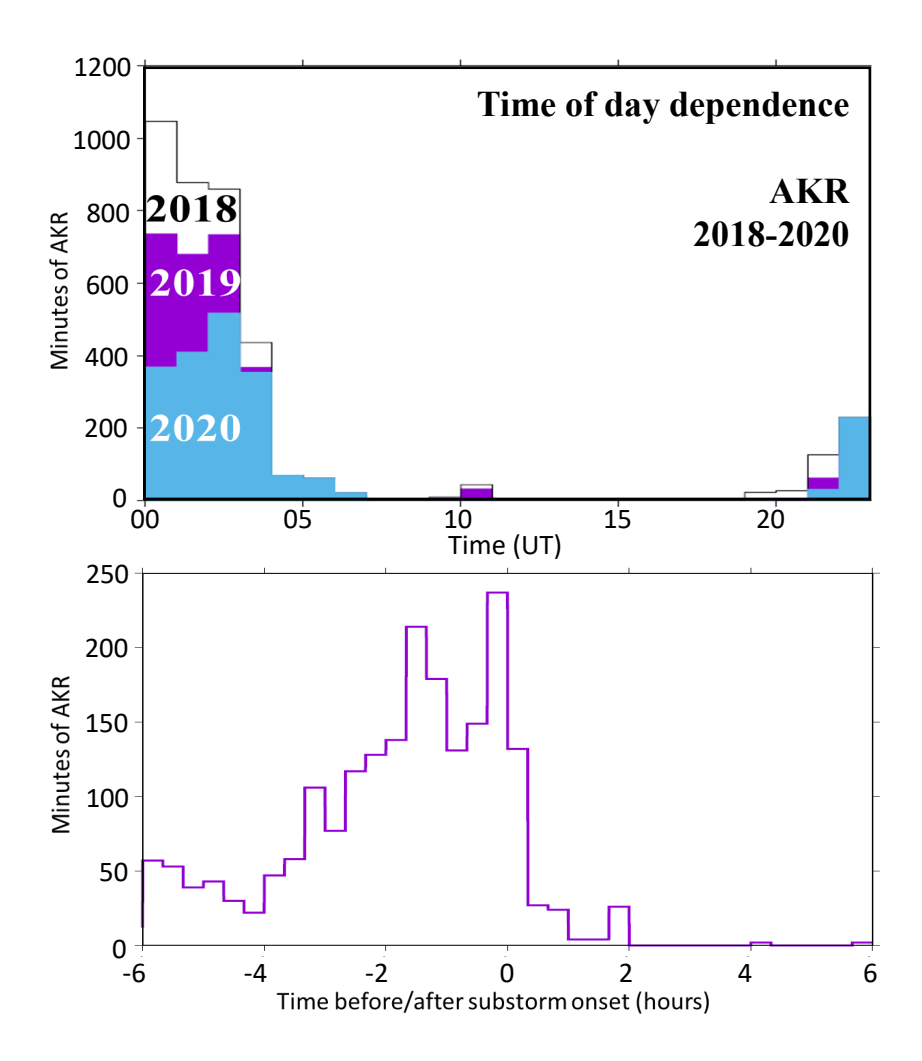


Figure 2: (a) Time of day distribution of leaked AKR observed at South Pole Station in 2018–2020. Leaked AKR occurs primarily between 2300–0400 UT corresponding to premidnight/midnight MLT. (b) Superposed epoch analysis of occurrence of leaked AKR at South Pole relative to substorm onsets identified from magnetometer data in the conjugate hemisphere.

& Alexander, 1977). The ground-level leaked AKR distribution corresponds to the high frequency end of the escaping AKR distribution. Assuming generation at the local electron cyclotron frequency, the leaked AKR comes from the lower part of the range of source heights that cause escaping AKR. Figure 3b shows the electron cyclotron frequency  $f_{ce}$  as function of altitude above South Pole, determined from the Definite/International Geomagnetic Reference Field (DGRF/IGRF) models (Gustafsson et al., 1992). Assuming generation at the electron cyclotron frequency, the observed primary frequency range 400-600 kHz corresponds to the altitude range 2500-3500 km. It is perhaps not surprising that the lowest altitude sources would have an easier time illuminating low altitudes if leaked AKR is generated in close proximity to the sources of escaping AKR, for example due to spreading out of the energy over propagation distance. However, DEMETER satellite observations of the frequency distribution of AKRlike emissions in the ionosphere do not show the effect seen at ground level but rather demonstrate a frequency distribution nearly identical to that of escaping AKR (Parrot et al., 2022). This brings up the possibility that the truncated distribution observed at ground level results not strictly from distance to the sources but rather from some condition of penetration through the Earth-ionosphere boundary. This could be indirectly related to distance from the sources, if the wave normal angle at low altitude depends on propagation or scattering in some way that is dependent on the distance or wave frequencies.

Figure 4 shows the distribution of maximum radiance of leaked AKR events observed at South Pole during May-August 2020, determined according to the following method. First, the receiver used for these observations was calibrated by comparing received signal levels to a calibration reference tone of known amplitude, and folding in transfer functions of the electronics determined in the lab before the instrument was deployed. Time intervals containing AKR, called "events", were identified by manual inspection of spectrograms. Events containing auroral hiss, identified through manual inspection, were discarded from the data set. For each event, at each frequency, the background level was determined as the 33<sup>rd</sup> percentile of sliding 20-s windows ranked by mean value, and a background radiance distribution was determined from all the samples in the selected window. A scaling factor was determined as the ratio of the number of samples in the selected window within  $\sim 1$  dB of the mean to the number of samples in the entire event within the same radiance range. At each frequency, the background radiance distribution adjusted by this scaling factor was subtracted from the distribution of the entire event to effectively remove the background from the event distribution. These adjusted event distributions were summed over a selected frequency range, 500–600 kHz in the case of the distribution shown in Figure 4. Interference lines, identified as frequencies for which the median radiance in the sliding window selected as the background level exceeded by > 6 dB the minimum such median background radiance among all frequencies, were removed. For each event, the maximum radiance was defined as the highest radiance for which the adjusted event distribution exceeded ten samples, deemed low enough to signify a maximum observed level and high enough to have statistical confidence in that level. Figure 4 shows the number of events binned according to this definition of maximum radiance level.

The low end cutoff near  $5 \times 10^{-19}$  W/m²/Hz is the instrumental detection threshold due to noise level. The distribution falls off monotonically above this level. Therefore, the radiance distribution in Figure 4 may represent the tail of a distribution that peaks at a level below the detection threshold. Half of the events exceed  $1.5 \times 10^{-18}$  W/m²/Hz, and 12.5% of the events exceed  $10^{-17}$  W/m²/Hz. The strongest events exceed  $2 \times 10^{-16}$  W/m²/Hz. These radiances are approximately two orders of magnitude weaker than those measured in the ionosphere with the DEMETER satellite,  $6 \times 10^{-16}$  to  $6 \times 10^{-14}$  W/m²/Hz (Parrot et al., 2022), or with the PHAZE–II (Physics of Auroral Zone Electrons) sounding rocket,  $3 \times 10^{-14}$  W/m²/Hz (LaBelle et al., 1999). The large difference between the intensities observed in space and at ground level suggest that the wave–normal distribution in space is probably broad, such that

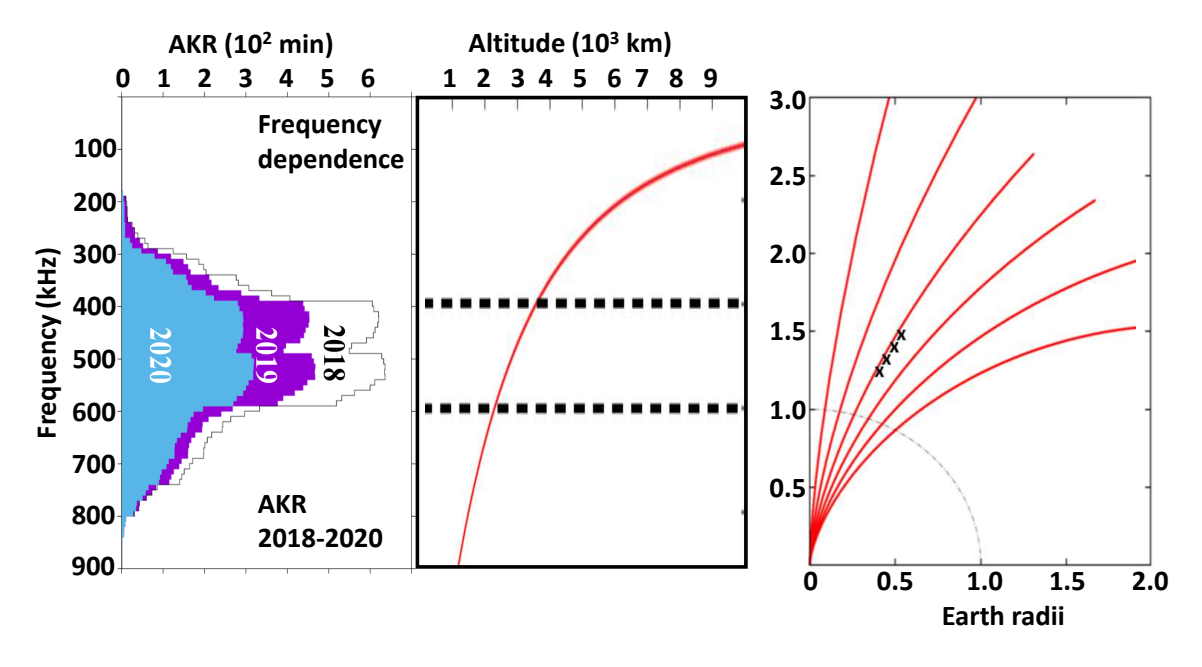


Figure 3: (a) Frequency distribution of leaked AKR observed at South Pole Station in 2018–2020. (b) Electron cyclotron frequency and sunrise/sunset times as a function of altitude above South Pole. (c) Depiction of possible source locations along the magnetic field lines.

only a tiny fraction of the waves fall within the transmission cone and penetrate the Earth–ionosphere boundary.

For reference, radiance of escaping AKR observed by distant satellites is significantly higher, for example  $10^{-14}$  W/m²/Hz at 25 R<sub>E</sub> (i.e.,  $1.6 \times 10^5$  km) in the original observations of Gurnett (1974). Assuming an upper bound of  $10^6$  km² for the area illuminated by leaked AKR, as suggested by simultaneous observations of leaked AKR at multiple Antarctic observatories (LaBelle et al., 2015), and assuming beam characteristics of escaping AKR described by Mutel et al. (2008), implies that the total radiated energy of escaping AKR is  $\sim 10^6$  times higher than that reaching ground level. The amount reaching the ionosphere may be two orders of magnitude higher as discussed above. In any case, if leaked AKR originates as Z-mode waves in close proximity and with comparable energy density to the escaping X-mode AKR, mode conversion and propagation may not need to be very efficient for those Z-mode waves to be the source of observed whistler mode leaked AKR.

# 3 Summary

For the first time, distributions of wave characteristics have been determined for leaked AKR observed at ground level, specifically at South Pole Station, Antarctica. These have been compared to distributions measured in the ionosphere with the DEMETER spacecraft (Parrot et al., 2022) and distributions of escaping AKR. South Pole observations of leaked AKR have frequency and day of year distributions different from those observed in the ionosphere with the DEMETER satellite, and have timing relative to substorm onsets different from that observed in escaping AKR. These discrepancies point to a major role of propagation conditions in determining the ground level distributions. The strict transmission—cone condition on the wave normal angle for penetration the Earth—ionosphere boundary is an obvious chief suspect in controlling ground—level leaked AKR, but other propagation effects such as ionospheric absorption and efficiency of sub—ionospheric propagation can also strongly influence whether leaked AKR is observed, and how strongly it is observed, at a ground station. Interpretations of these effects could benefit from simultaneous conjugate observations of AKR in the ionosphere and at ground level.

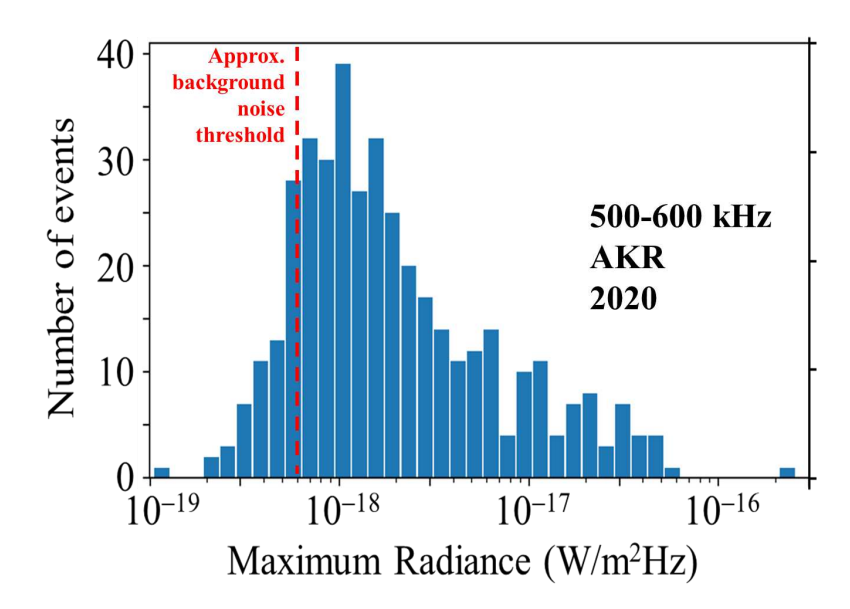


Figure 4: (a) Distribution of maximum radiance of leaked AKR observed at South Pole Station in 2020. The apparent cutoff at  $5 \times 10^{-19}$  W/m<sup>2</sup>/Hz is due to the instrument noise level. Half of the events exceed  $1.5 \times 10^{-18}$  W/m<sup>2</sup>/Hz.

# Acknowledgements

The authors thank Dartmouth engineers David McGaw and Terry Kovacs for supporting the South Pole instrumentation in 2018–2020, and the South Pole technicians for their help at the station. We acknowledge the substorm timing list identified by the Newell and Gjerloev technique (Newell & Gjerloev, 2011a), the SMU and SML indices (Newell & Gjerloev, 2011b); and the SuperMAG collaboration (Gjerloev, 2012). This study was supported by National Science Foundation grant ANT–2205753 to Dartmouth College.

### References

- Bilitza D., Altadill D., Truhlik V., Shubin V., Galkin I., Reinisch B., Huang X., 2017, International Reference Ionosphere 2016: From ionospheric climate to real-time weather predictions, *Space Weather*, 15, 418
- Chian A. C. L., Lopes S. R., Alves M. V., 1994, Generation of auroral whistler-mode radiation via nonlinear coupling of Langmuir waves and Alfven waves, Astronomy and Astrophysics, 290, L13
- Ergun R. E., Carlson C. W., McFadden J. P., Delory G. T., Strangeway R. J., Pritchett P. L., 2000, Electron-Cyclotron Maser Driven by Charged-Particle Acceleration from Magnetic Field-aligned Electric Fields, *The Astrophysical Journal*, 538, 456
- Fogg A. R., Jackman C. M., Waters J. E., Bonnin X., Lamy L., Cecconi B., Issautier K., Louis C. K., 2022, Wind/WAVES Observations of Auroral Kilometric Radiation: Automated Burst Detection and Terrestrial Solar Wind - Magnetosphere Coupling Effects, Journal of Geophysical Research (Space Physics), 127, e30209
- Gjerloev J. W., 2012, The SuperMAG data processing technique, Journal of Geophysical Research (Space Physics), 117, A09213
- Gurnett D. A., 1974, The Earth as a radio source: Terrestrial kilometric radiation, *Journal of Geophysical Research*, 79, 4227
- Gustafsson G., Papitashvili N. E., Papitashvili V. O., 1992, A revised corrected geomagnetic coordinate system for Epochs 1985 and 1990., *Journal of Atmospheric and Terrestrial Physics*, 54, 1609
- Kaiser M. L., Alexander J. K., 1977, Terrestrial kilometric radiation, 3. Average spectral properties, Journal of Geophysical Research, 82, 3273
- Krasovskiy V. L., Kushnerevskiy Y. V., Mugulin V. V., Orayevskiy V. N., Pulinets S. A., 1983, Ballistic wave transformation as a mechanism for the linkage of terrestrial kilometric radio waves with low frequency noise in the upper atmosphere, *Geomagnetism and Aeronomy*, 23, 702
- LaBelle J., Anderson R. R., 2011, Ground-level detection of auroral kilometric radiation, Geophysical Research Letters, 38, L04104
- LaBelle J., McAdams K. L., Trimpi M. L., 1999, High-frequency and time resolution rocket observations of structured low- and medium-frequency whistler mode emissions in the auroral ionosphere, *Journal* of Geophysical Research, 104, 28101
- LaBelle J., et al., 2015, Further evidence for a connection between auroral kilometric radiation and ground-level signals measured in Antarctica, *Journal of Geophysical Research (Space Physics)*, 120, 2061
- LaBelle J., Yearby K., Pickett J. S., 2022, South Pole Station Ground-Based and Cluster Satellite Measurements of Leaked and Escaping Auroral Kilometric Radiation, *Journal of Geophysical Research* (Space Physics), 127, e2021JA029399

- Liou K., Meng C. I., Lui A. T. Y., Newell P. T., Anderson R. R., 2000, Auroral kilometric radiation at substorm onset, *Journal of Geophysical Research*, 105, 25325
- Morioka A., Oya H., Miyaoka H., Ono T., Obara T., 1988, Wave-particle interaction in the auroral ionosphere in LF and HF range Results from Antarctic rocket observations, *Journal of Geomegaetism and Geoelectricity*, 40, 923
- Morioka A., et al., 2007, Dual structure of auroral acceleration regions at substorm onsets as derived from auroral kilometric radiation spectra, Journal of Geophysical Research (Space Physics), 112, A06245
- Morioka A., et al., 2011, On the simultaneity of substorm onset between two hemispheres, *Journal of Geophysical Research (Space Physics)*, 116, A04211
- Morioka A., Miyoshi Y., Kasaba Y., Sato N., Kadokura A., Misawa H., Miyashita Y., Mann I., 2014, Substorm onset process: Ignition of auroral acceleration and related substorm phases, *Journal of Geophysical Research (Space Physics)*, 119, 1044
- Mutel R., Gurnett D., Christopher I., 2004, Spatial and temporal properties of AKR burst emission derived from Cluster WBD VLBI studies, *Annales Geophysicae*, 22, 2625
- Mutel R. L., Christopher I. W., Pickett J. S., 2008, Cluster multispacecraft determination of AKR angular beaming, *Geophysical Research Letters*, 35, L07104
- Mutel R. L., Christopher I. W., Menietti J. D., Gurnett D. A., Pickett J. S., Masson A., Fazakerley A., Lucek E., 2011, RX and Z Mode Growth Rates and Propagation at Cavity Boundaries, in Planetary, Solar and Heliospheric Radio Emissions (PRE VII), eds Rucker, H. O. and Kurth, W. S. and Louarn, P. and Fischer, G., pp 241–252
- Newell P. T., Gjerloev J. W., 2011a, Evaluation of SuperMAG auroral electrojet indices as indicators of substorms and auroral power, *Journal of Geophysical Research (Space Physics)*, 116, A12211
- Newell P. T., Gjerloev J. W., 2011b, Substorm and magnetosphere characteristic scales inferred from the SuperMAG auroral electrojet indices, *Journal of Geophysical Research (Space Physics)*, 116, A12232
- Oya H., Miyaoka H., Miyatake S., 1979, Observation of HF plasma wave emissions at ionospheric level using sounding rockets S-210JA-1, 2 in Antarctica, Antarctic Record, 64, 30
- Oya H., Morioka A., Obara T., 1985, Leaked AKR and terrestrial hectometric radiations discovered by the plasma wave and planetary plasma sounder experiments on board the Ohzora (EXOS-C) satellite Instrumentation and observation results of plasma wave phenomena, *Journal of Geomagnetism and Geoelectricity*, 37, 237
- Parrot M., Berthelier J.-J., 2012, AKR-like emissions observed at low altitude by the DEMETER satellite, Journal of Geophysical Research (Space Physics), 117, A10314
- Parrot M., Němec F., Santolík O., 2022, Properties of AKR-Like Emissions Recorded by the Low Altitude Satellite DEMETER During 6.5 Years, Journal of Geophysical Research (Space Physics), 127, e30495
- Pritchett P. L., Strangeway R. J., Carlson C. W., Ergun R. E., McFadden J. P., Delory G. T., 1999, Free energy sources and frequency bandwidth for the auroral kilometric radiation, *Journal of Geophysical Research*, 104, 10317
- Shutte N., Prutensky I., Pulinets S., Kløos Z., Rothkaehl H., 1997, The charged-particle fluxes at auroral and polar latitudes and related low-frequency auroral kilometric radiation-type and high-frequency wideband emission, *Journal of Geophysical Research*, 102, 2105
- Treumann R. A., 2006, The electron-cyclotron maser for astrophysical application, *The Astronomy and Astrophysics Review*, 13, 229

- Waters J. E., et al., 2022, A Perspective on Substorm Dynamics Using 10 Years of Auroral Kilometric Radiation Observations From Wind, Journal of Geophysical Research (Space Physics), 127, e30449
- Wu C. S., Yoon P. H., Freund H. P., 1989, A theory of electron cyclotron waves generated along auroral field lines observed by ground facilities, *Geophysical Research Letters*, 16, 1461
- Xiao F., et al., 2022, Asymmetric Distributions of Auroral Kilometric Radiation in Earth's Northern and Southern Hemispheres Observed by the Arase Satellite, Geophysical Research Letters, 49, e99571
- Ziebell L. F., Wu C. S., Yoon P. H., 1991, Kilometric radio waves generated along auroral field lines observed by ground facilities: A theoretical model, *Journal of Geophysical Research*, 96, 1495